Silicone Oil Affects Fibrosis of Human Trabecular Meshwork Cells by Upregulating Ferroptosis Through a ROS/NOX4/Smad3 Axis

Jing Wang,[1] Yang Zhang,[1] Huimin Zhong,[2] Yumeng Zhang,[1] Ruiqi Han,[1] Yanzhi Guo,[1] Shouyue Huang,[1] Huan Yu,[1] and Yisheng Zhong[1]

[1]Department of Ophthalmology, Ruijin Hospital Affiliated Medical School, Shanghai Jiaotong University, Shanghai, China
[2]Department of Ophthalmology, Shanghai General Hospital (Shanghai First People's Hospital), Shanghai Jiao Tong University School of Medicine, Shanghai, China

Correspondence: Yisheng Zhong, Department of Ophthalmology, Ruijin Hospital Affiliated Medical School, Shanghai Jiaotong University, 197 Ruijin Er Rd., Shanghai 200025, China; yszhong68@126.com.
Huan Yu, Department of Ophthalmology, Ruijin Hospital Affiliated Medical School, Shanghai Jiaotong University, 197 Ruijin Er Rd., Shanghai 200025, China; yuhuan0828@outlook.com.
Shouyue Huang, Department of Ophthalmology, Ruijin Hospital Affiliated Medical School, Shanghai Jiaotong University, 197 Ruijin Er Rd., Shanghai 200025, China; yachtjj@hotmail.com.

JW, YZ, and HZ contributed equally and should therefore be regarded as equivalent authors.

Received: June 24, 2024
Accepted: February 17, 2025
Published: March 11, 2025

Citation: Wang J, Zhang Y, Zhong H, et al. Silicone oil affects fibrosis of human trabecular meshwork cells by upregulating ferroptosis through a ROS/NOX4/Smad3 axis. *Invest Ophthalmol Vis Sci.* 2025;66(3):25. https://doi.org/10.1167/iovs.66.3.25

Purpose. Silicone oil (SiO) is commonly employed as an intravitreal tamponade to manage complex retinal detachments associated with proliferative diabetic retinopathy, trauma, or severe myopia and to facilitate retinal reattachment. Nevertheless, SiO usage is linked to several complications, notably secondary glaucoma, which constitutes a significant proportion of adverse effects. This study investigated the impact of SiO on trabecular meshwork cells, given their pivotal role in regulating aqueous humor outflow.

Methods. Human trabecular meshwork cells (HTMCs) were co-cultured with SiO. The impact on proliferation, fibrosis-related markers, and ferroptosis levels on these cells was evaluated using 5-ethynyl-2′-deoxyuridine (EdU), western blot, and immunofluorescence assays. Further gene knockdown experiments with NOX4 and Smad3 were conducted to elucidate the underlying mechanisms of SiO-induced changes.

Results. SiO intervention inhibited HTMC proliferation, upregulated fibrosis-related markers, and elevated ferroptosis levels. Gene knockdown experiments revealed that SiO-induced ferroptosis and reactive oxygen species (ROS) increase were mediated through NOX4 upregulation and Smad3 activation.

Conclusions. These findings highlight the significance of ferroptosis and the ROS/NOX4/Smad3 axis in the mechanism of SiO-induced intraocular pressure elevation. The insights gained from this study identify potential therapeutic targets to mitigate postoperative complications associated with SiO tamponade in ophthalmic surgery.

Keywords: silicone oil, trabecular meshwork cells, ferroptosis, ROS/NOX4/Smad3 axis

Silicone oil (SiO) possesses the capability to displace aqueous humor from the retinal surface, thereby maintaining the adhesion between the retina and retinal pigment epithelium.[1] Since its introduction into ophthalmic surgery by Cibis et al. in 1962,[2] SiO has become a staple for intraocular tamponade following pars plana vitrectomy (PPV). It has proven beneficial in managing proliferative vitreoretinopathy and extensive tractional retinal detachments associated with proliferative diabetic retinopathy.[3–5] Furthermore, in the treatment of ocular trauma, SiO has been effective in minimizing the risk of postoperative bleeding, ensuring retinal attachment, and preventing phthisis in cases of severely traumatized eyes.[6]

However, there are also reports indicating that vitreous filling with SiO is closely linked to postoperative complications such as keratopathy, cataract, and glaucoma.[7] Among these, increased intraocular pressure (IOP) is one of the most frequent complications following the use of SiO in the vitreous cavity. The mechanisms proposed include pupillary block, postoperative inflammation, and migration of SiO into the anterior chamber.[8,9] In clinical situations, if a patient is unable to maintain a prone position after surgery, the lower density of SiO may cause it to migrate toward the upper part of the eye, nearing the lens and potentially diffusing into the anterior chamber. This migration can result in mechanical obstruction to aqueous humor filtration.[10] Further-

more, the presence of SiO in the anterior chamber leading to extensive infiltration of the trabecular meshwork is another potential cause of elevated IOP following PPV.[11–14] However, The pathogenesis of increased IOP due to the migration of SiO into the anterior chamber remains poorly understood.

It is well known that dysfunction of trabecular meshwork cells (TMCs) is a critical factor in the pathogenesis of primary open-angle glaucoma (POAG).[15] The trabecular meshwork, a key structure in the anterior chamber, is responsible for regulating aqueous humor outflow.[16] When the ability of the trabecular meshwork to regulate outflow is compromised, drainage efficiency decreases, leading to elevated IOP.[17] TMCs are crucial for maintaining the structure and function of the trabecular meshwork, primarily through the production and remodeling of the extracellular matrix (ECM), which provides the structural framework of the meshwork.[18] In cases of glaucoma, dysregulation of TMC activity can result in the accumulation of excessive ECM material, thereby increasing resistance to aqueous humor outflow.[19]

Ferroptosis represents a metabolically orchestrated form of cell demise propelled by iron ion–dependent lipid peroxidation, manifesting in compromised cell membrane integrity and subsequent cytoplasmic content leakage.[20,21] Its regulatory network encompasses intricate pathways concerning iron metabolism,[22] lipid metabolism,[23] and the modulation of antioxidant signaling cascades.[24] The implication of ferroptosis in diverse pathogenic processes, including but not limited to oncogenesis, ischemia–reperfusion injury, and neurodegenerative maladies, has been extensively documented.[21,25,26] Within the domain of ophthalmology, scholarly discourse has posited a nexus between ferroptosis and glaucomatous pathology.[27,28] Investigations have elucidated the pivotal role of iron homeostasis in governing the health of the optic nerve and retinal ganglion cells.[29–31] Furthermore, perturbed metal equilibrium and heightened oxidative stress within the trabecular meshwork constitute notable observations in glaucomatous conditions.[32–34] Notably, oxidative stress, a cardinal downstream consequence of ferroptosis, emerges as a pivotal determinant in cellular senescence, thereby assuming a critical role in the etiopathogenesis and predisposition to glaucoma.[35,36]

Building upon these insights, we postulated that the introduction of SiO elicits alterations in ferroptosis within TMCs, consequently modulating their fibrotic propensity, which plausibly contributes to the observed elevation in IOP subsequent to PPV employing SiO. To scrutinize this conjecture, we conducted an assessment encompassing the biomechanical attributes and ferroptotic indices of human trabecular meshwork cells (HTMCs) alongside their ECM following SiO intervention. Additionally, we embarked on an inquiry into the specific mechanistic underpinnings and associated signaling cascades governing these phenomena.

Materials and Methods

Culture of Cells With SiO

Primary HTMCs were obtained from ScienCell Research Laboratories (6590; Carlsbad, CA, USA). Donor age and gender are provided in Table 1, and no history of ocular disease was reported for any donor. All experiments were performed in triplicate using cells from three independent donors. HTMCs were cultured in Gibco Minimum Essential Medium (Thermo Fisher Scientific, Waltham, MA, USA) supplemented with 10% fetal bovine serum (FBS), antibiotics (100 U/mL penicillin + 100 µg/mL streptomycin), and antimycotics (0.25 µg/mL amphotericin B). The cells were incubated in a humidified environment with 5% CO_2 at 37°C. The culture medium was refreshed 48 hours after initial plating. The cells underwent passaging through trypsinization and were utilized for experiments between the second and fourth passages.

Table 1. HTMC Donors

HTMC Donor	Sex	Age (y)
1	Male	59
2	Female	62
3	Male	37

For western blot and quantitative real-time polymerase chain reaction (qRT-PCR) experiments, TMCs were inoculated in the lower chamber of Transwell six-well plates (Corning Inc., Corning, NY, USA), and SiO was applied to the upper chamber. In contrast, for immunofluorescence (IF) and 5-ethynyl-2′-deoxyuridine (EdU) assays, HTMCs were seeded in 24-well plates, where a slide was pre-placed and SiO was directly added to the culture medium. For Cell Counting Kit-8 (CCK-8) assays, HTMCs were inoculated in 96-well plates, with SiO again directly added to the culture medium. In all experiments, the duration of SiO treatment was maintained at 48 hours. The SiO used in this study (Oxane 5700) was obtained from Bausch & Lomb (Bridgewater, NJ, USA). The viscosity of the silicone oil was 5000 to 5900 mPa·s. The concentration of SiO was determined by the volume ratio of SiO to the culture medium in the cell culture dish.

EdU Assay

HTMCs were seeded at a density of 5×10^4 cells/well in 24-well plates with pre-placed slides and treated with SiO at concentrations of 0%, 5%, 10%, 20%, and 40% for 48 hours. Then, the HTMCs were incubated with 50-mM EdU medium diluent (RiboBio, Guangzhou, China) in 24-well plates for 3 hours to facilitate the incorporation of EdU into newly synthesized DNA. After incubation, the cells were fixed and permeabilized, followed by a 30-minute reaction with 100 µL of 1× Apollo reaction cocktail (RiboBio) to visualize the incorporated EdU. Cell nuclei were then stained with Hoechst 33342 (Solarbio, Beijing, China) to facilitate visualization of all nuclei.

EdU-positive cells, indicating active DNA synthesis, were imaged using fluorescence microscopy (Carl Zeiss Microscopy, Oberkochen, Germany). Images captured were subsequently analyzed with ImageJ (National Institutes of Health, Bethesda, MD, USA) to quantify the proportion of cells undergoing DNA synthesis, providing insights into cellular proliferation rates.

CCK-8 Assay

HTMCs were seeded at a density of 1×10^4 cells/well in 96-well plates and treated with SiO at concentrations of 0%, 5%, 10%, 20%, and 40% for 48 hours. The culture medium was then replaced with 90 µL of fresh medium, followed by

Table 2. Gene Primer Sequences

Gene	Forward Sequence	Reverse Sequence
β-actin	CACTATCGGCAATGAGCGGTTCC	CAGCACTGTGTTGGCATAGAGGTC
NOX4	ACTGCCTCCATCAAGCCAAGATTC	CTCCAGCCACACACAGACTAACTTC
COX2	CAATGGGCTGGAAGACATATCA	GCCAGGGCTGAACTTCGAA
Ferritin	CCATCAACCGCCAGATCAACCTG	GTTTCTCAGCATGTTCCCTCTCCTC
GPX4	CCGCTGTGGAAGTGGATGAAGATC	CTTGTCGATGAGGAACTGTGGAGAG

the addition of 10 µL of CCK-8 solution to each well. After a 1-hour incubation at 37°C, optical density was measured at 450 nm using an ELISA microplate reader (ELX800; BioTek, Winooski, VT, USA).

Western Blotting

Protein extraction was conducted when cell confluence reached approximately 80%. Cells were lysed in RIPA Lysis Buffer (Sigma-Aldrich, St. Louis, MO, USA) supplemented with a cocktail of protease inhibitors (1% phenylmethylsulfonyl fluoride + 1% phosphorylase inhibitors) on ice. Proteins were quantified (20 µg), and equal amounts (10 µL) were separated on 10% polyacrylamide gels, followed by electrotransfer onto polyvinylidene fluoride membranes (Merck Millipore, Billerica, MA, USA). The membranes were blocked for 2 hours in Tris-buffered saline with 0.1% Tween 20 (TBST) containing 5% fat-free milk. They were then incubated overnight at 4°C with primary antibodies diluted in TBST containing 3% bovine serum albumin. After washing, the membranes were incubated with horseradish peroxidase (HRP)-conjugated secondary antibodies for 1 hour at room temperature. Antigen–antibody complexes were visualized using a chemiluminescence reagent kit (Thermo Fisher Scientific).

The densities of the bands were scanned using a VersaDoc imaging system (Bio-Rad Laboratories, Hercules, CA, USA) and analyzed with Image Pro Plus 6.0 (Media Cybernetics, Rockville, MD, USA). Data are expressed as the ratio of the protein of interest to glyceraldehyde 3-phosphate dehydrogenase (GAPDH) in the same sample, facilitating relative quantification of protein expression.

The primary antibodies were anti-GAPDH (ab8245, 1:10,000 dilution; Abcam, Cambridge, UK), anti-fibronectin (ab2413, 1:1000 dilution; Abcam), anti-myocilin (ab41552, 1:1000 dilution; Abcam), anti-alpha-smooth muscle actin (α-SMA; ab7817, 1:1000 dilution; Abcam), anti-acyl-CoA synthetase long-chain family member 4 (ACSL4; ab155282, 1:5000 dilution; Abcam), anti-cyclooxygenase-2 (COX2; ab179800, 1:1000 dilution; Abcam), anti-glutathione peroxidase 4 (GPX4; ab125066, 1:1000 dilution; Abcam), and anti-ferritin (ab75973, 1:1000 dilution; Abcam). The secondary antibodies were Goat Anti-Rabbit IgG H&L (HRP) (ab6721, 1:10,000 dilution; Abcam), and Rabbit Anti-Mouse IgG H&L (HRP) (ab6728, 1:5000 dilution; Abcam).

Immunohistochemistry

The HTMCs were fixed in 4% paraformaldehyde for 30 minutes at room temperature and subsequently washed in PBS to remove any residual mucus layer. The cells were then blocked and incubated overnight with primary antibodies at 4°C. Following this, the samples were incubated with donkey anti-rabbit IgG (1:1000 dilution; Abcam) or phalloidin (1:1000 dilution; Abcam) at room temperature for 1 hour. Cells were further stained with 4′,6-diamidino-2-phenylindole (DAPI; Sigma-Aldrich) for 5 minutes to label nuclei and then examined under a microscope (Carl Zeiss Microscopy).

For post-acquisition processing, Photoshop (Adobe, San Jose, CA, USA) was utilized to uniformly adjust the brightness and contrast of the images. Cell height was quantified using ImageJ software. This approach ensured consistent, reproducible image analysis while minimizing potential biases in visualization and measurement.

Transfection of siRNA

NADPH oxidase 4 (NOX4) expression was silenced using NOX4-specific small interfering RNA (siRNA; Life Technologies, Carlsbad, CA, USA). Cells were plated in 24-well plates with medium containing 10% FBS and allowed to grow for 24 hours until they reached approximately 80% confluency. Subsequently, 50-nM siRNA (target sequence: F, 5′-UGUUUAACCCCUUCGUUGGCG-3′; R, 5′-CCAACGAAGGGGUUAAACACC-3′) was complexed with Invitrogen Lipofectamine 3000 (Thermo Fisher Scientific) following the manufacturer's instructions and administered to the cells. The experiment included four groups: a blank group (no treatment), a liposome group (vehicle control), a non-targeting siRNA group (negative control), and a targeting siRNA group (test group). After 24 hours of treatment, cells were harvested, and RNA was extracted for subsequent analysis.

Quantitative Real-Time PCR

RNA extraction was performed when cell confluence reached approximately 80%. Total RNA was extracted from HTMCs utilizing Invitrogen TRIzol Reagent in accordance with the manufacturer's guidelines. The isolated RNA was subsequently reverse transcribed into complementary DNA (cDNA) using the PrimeScript RT Master Mix kit (Takara Bio, Shiga, Japan). Primer sequences were designed utilizing Primer Premier 5.0 software, and the specific primer pairs utilized are shown in Table 2.

Quantitative real-time PCR amplification was conducted using the SYBR Premix Ex Taq II kit (Takara Bio) in a total reaction volume of 20 µL on a 7500 real-time PCR system (Applied Biosystems, Foster City, CA). The amplification protocol consisted of an initial denaturation step at 95°C for 30 seconds, followed by 40 cycles of denaturation at 95°C for 5 seconds, annealing at 60°C for 34 seconds, and extension at 72°C for 30 seconds. Duplicate measurements were performed for each sample to ensure accuracy. β-Actin was utilized as an internal reference gene for normalization

Investigative Ophthalmology & Visual Science

purposes. The relative expression levels of each target gene were determined using the $2^{-\Delta\Delta Ct}$ method, as previously described.[37]

Statistical Analysis

Statistical analyses were conducted using SPSS Statistics 19.0 (IBM, Chicago, IL, USA). All results are expressed as mean ± SD. Data were analyzed using a Student's *t*-test or a one-way ANOVA test. $P < 0.05$ was considered statistically significant. For graphical representation of the data, Prism 6.04 (GraphPad Software, Boston, MA, USA) was utilized.

Results

SiO Modulates Proliferation and Upregulates Fibrosis-Related Markers in HTMCs

To investigate the impact of SiO on the proliferation of HTMCs, the cells were co-cultured with varying concentrations of SiO (5%, 10%, 15%, 20%) for a duration of 48 hours. The EdU incorporation assays revealed a concentration-dependent decrease in the proliferation rate of HTMCs (Fig. 1A). The results of the CCK-8 assay demonstrated a gradual decrease in HTMC viability with increasing SiO concentration (Fig. 1B). Concurrently, we assessed the expression of fibrosis-associated proteins (fibronectin,

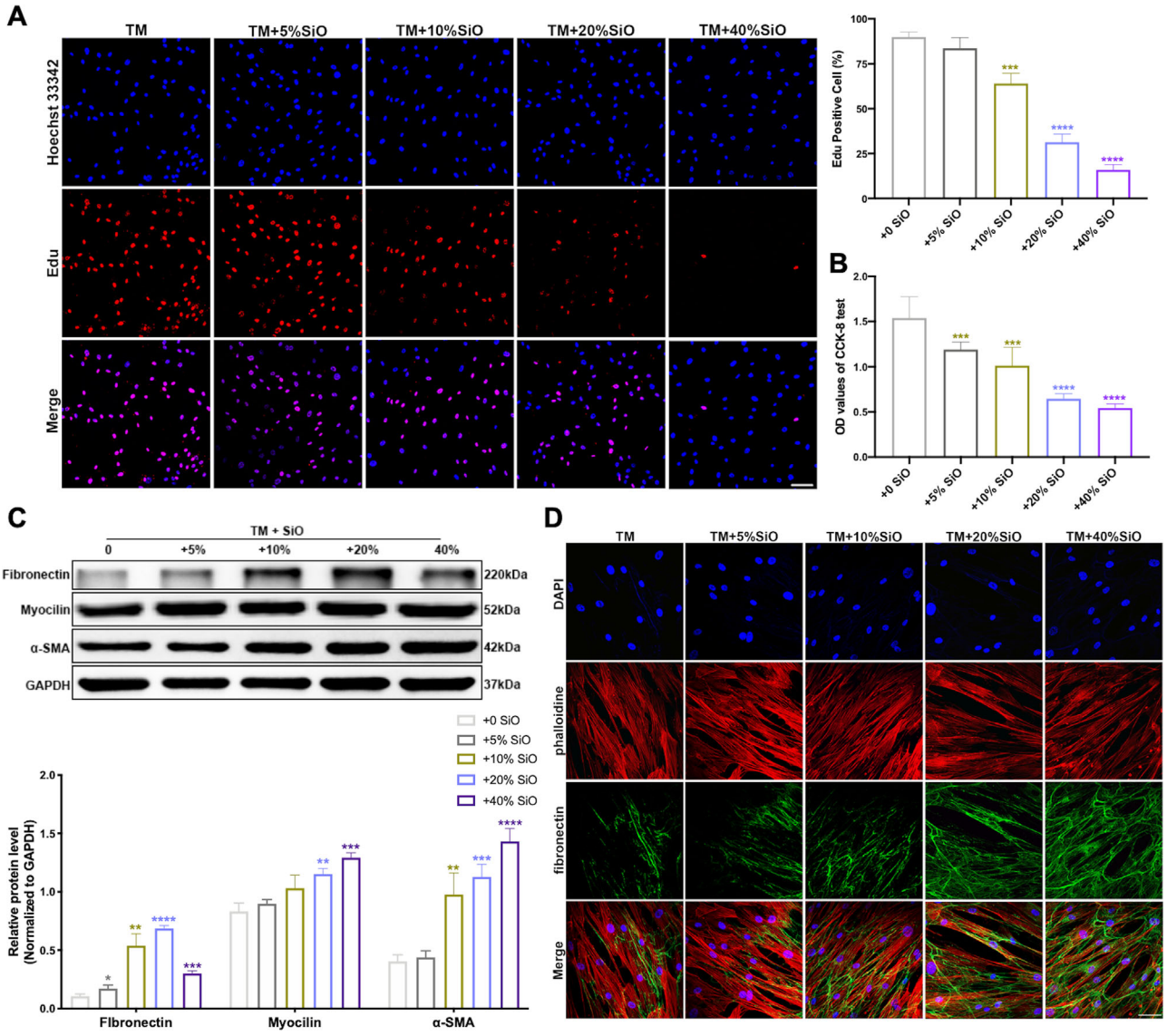

Figure 1. Changes in proliferation and viability of HTMCs and fibronectin, myocilin, and α-SMA expression within HTMCs when co-cultured with SiO. (**A**) EdU test detected the proliferation of TMCs. Results indicated a progressive decline in cell proliferation with increasing SiO concentrations, reaching a minimum ($P < 0.0001$) at a concentration of 40% SiO ($n = 3$). Magnification, 100×. *Scale bar*: 25 µm. (**B**) CCK-8 test detected the viability of TMCs. Results demonstrated a gradual decline in cell viability with increasing concentrations of SiO, reaching the lowest viability ($P < 0.0001$) at a concentration of 40% SiO ($n = 3$). (**C**) Protein expression of fibronectin, myocilin, and α-SMA in HTMCs co-cultured with different concentrations of SiO. Fibronectin ($P < 0.0001$) expression peaked at a SiO concentration of 20%, and myocilin ($P = 0.0005$) and α-SMA ($P < 0.0001$) reached maximum expression at a SiO concentration of 40% ($n = 3$). (**D**) Labeling of fibronectin in HTMCs co-cultured with SiO. Representative images depict the immunohistochemistry for HTMCs labeled by DAPI (*blue*), phalloidin (*red*), and fibronectin (*green*). Magnification, 200×. *Scale bar*: 25 µm. *$P < 0.05$, **$P < 0.01$, ***$P < 0.001$, ****$P < 0.0001$ versus the control group.

Investigative Ophthalmology & Visual Science

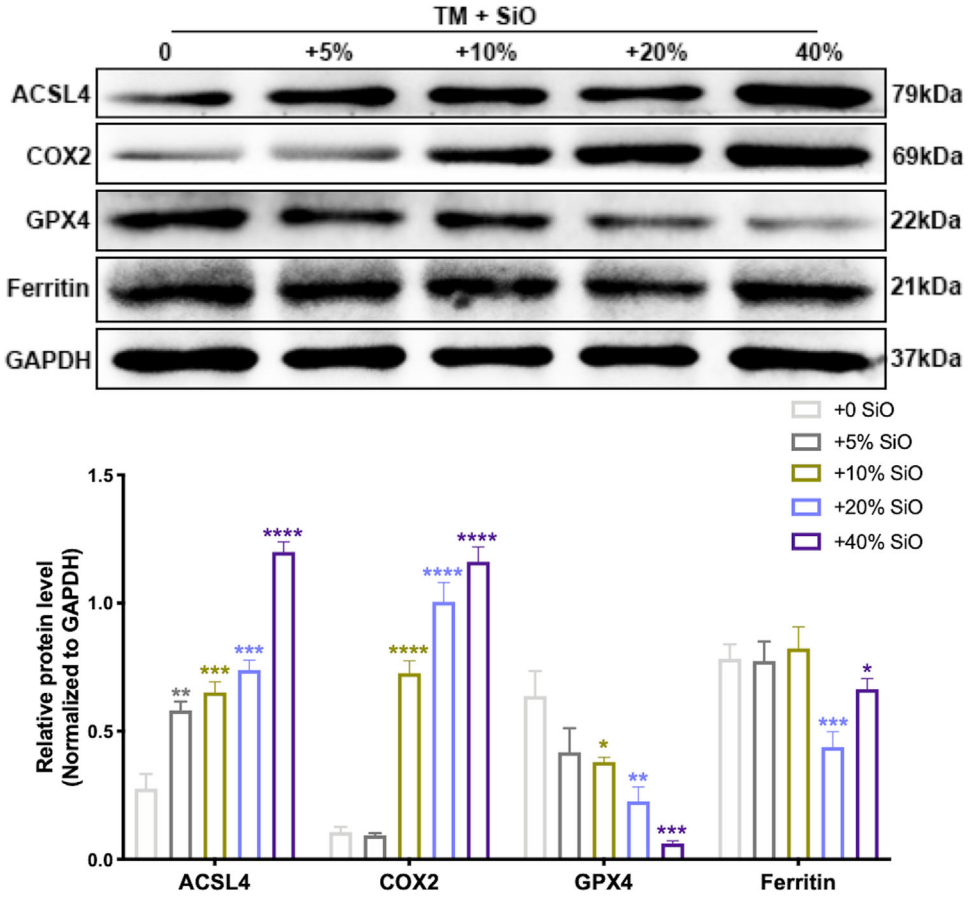

Figure 2. Protein expression of ACSL4, COX2, GPX4, and ferritin in HTMCs co-cultured with different concentrations of SiO. Expression levels of ACSL4 and COX2 increased progressively with rising SiO concentrations, reaching their highest levels at 40% SiO ($P < 0.0001$). Conversely, GPX4 and ferritin expression levels decreased as SiO concentration increased, with GPX4 ($P = 0.0005$) reaching its lowest expression at 40% SiO and ferritin ($P = 0.0003$) at 20% SiO ($n = 3$). *$P < 0.05$, **$P < 0.01$, ***$P < 0.001$, ****$P < 0.0001$ versus the control group.

myocilin, and α-SMA) in HTMCs post co-culture with SiO. Western blot analysis indicated that the levels of fibronectin, myocilin, and α-SMA increased progressively with higher concentrations of SiO (Fig. 1C). This suggests a significant role of SiO in promoting fibrosis in HTMCs. Additionally, IF staining experiments provided a more direct visualization, showing a marked increase in the fluorescence intensity of fibronectin in HTMCs after co-culture with SiO (Fig. 1D). These findings collectively suggest that SiO not only inhibits the proliferation but also enhances the fibrotic response in HTMCs.

SiO Upregulates Ferroptosis Level in HTMCs

To further understand the impact of SiO on TMCs, we assessed its effects on the ferroptotic pathway in HTMCs. HTMCs were co-cultured with varying concentrations of SiO, and the expression of key ferroptosis markers was examined. Western blot analysis revealed that, as SiO concentration increased, the expression of pro-ferroptotic proteins ACSL4 and COX2 also increased. Conversely, the expression of GPX4 and ferritin, both of which are protective against ferroptosis, decreased. These changes suggest that SiO may enhance the ferroptotic process in HTMCs, and this effect appears to be dose dependent (Fig. 2). These data highlight a potential mechanism by which SiO could influence TMC viability and function, further supporting the hypothesis that the role of SiO in ocular complications may involve the induction of ferroptosis in HTMCs.

Exploring the Relationship Between Ferroptosis and Fibrosis in HTMCs After SiO Exposure

The current experimental results demonstrated that SiO intervention affected the fibrosis and changed the level of ferroptosis in HTMCs. Accordingly, we speculated that the effect of SiO on HTMC fibrosis might be achieved by increasing the ferroptosis level. To test this hypothesis, HTMCs pretreated with 20% SiO were subjected to either ferroptosis inducers (erastin) or inhibitors (ferrostatin-1 [Fer-1]), and the subsequent effects on fibrosis were assessed. Initially, the efficacy of the ferroptosis modulators was established through western blot analysis, which demonstrated expected changes in ferroptosis markers following treatment with erastin or Fer-1 in SiO-pretreated HTMCs (Fig. 3A). IF staining revealed that erastin significantly reduced ferritin fluorescence, whereas Fer-1 increased it, indicating successful modulation of ferropto-

Investigative Ophthalmology & Visual Science

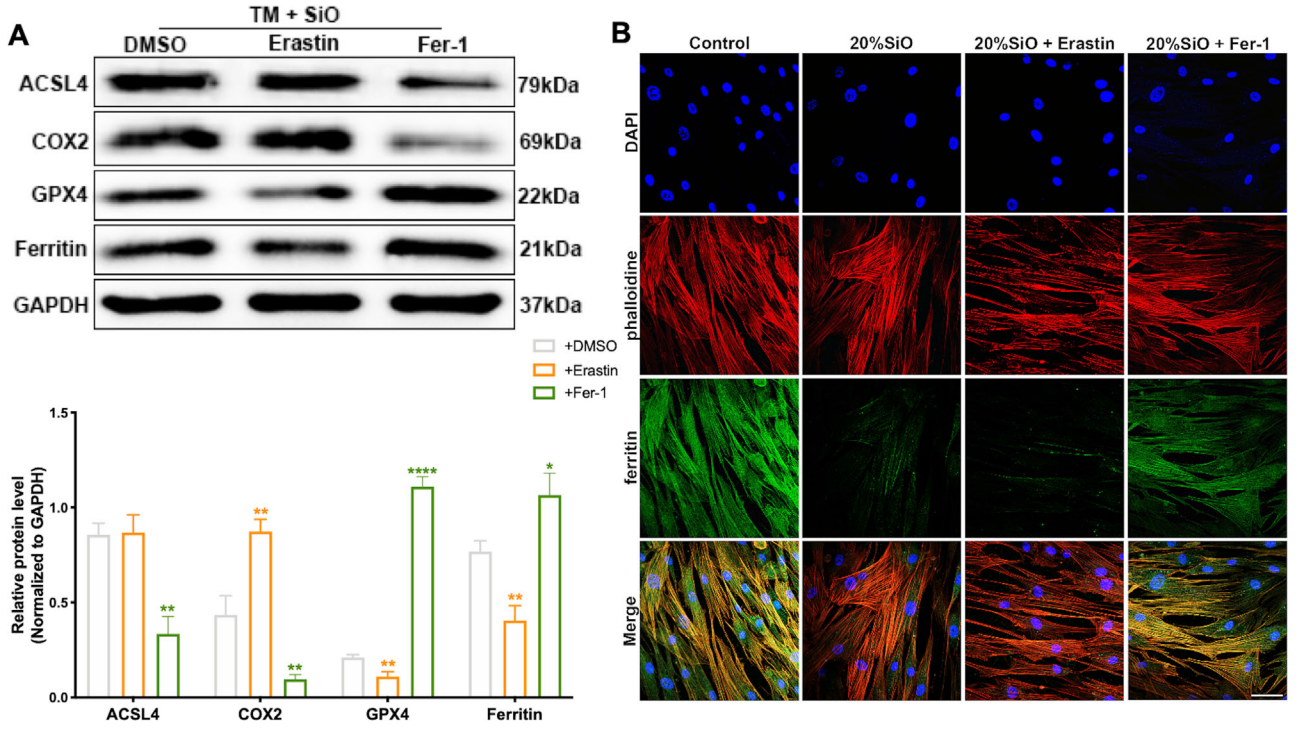

Figure 3. Effects of inducers (erastin) or inhibitors (Fer-1) of ferroptosis on ferroptosis-related indicators. (**A**) Protein expression of ACSL4 ($P = 0.8599$ and $P = 0.0012$), COX2 ($P = 0.0015$ and $P = 0.0024$), GPX4 ($P = 0.0045$ and $P < 0.0001$), and ferritin ($P = 0.0029$ and $P = 0.0164$) in HTMCs treated with SiO and erastin/Fer-1, respectively ($n = 3$). (**B**) Labeling of ferritin in HTMCs treated with SiO and erastin/Fer-1. Representative images depict the immunohistochemistry for HTMCs labeled by DAPI (*blue*), phalloidin (*red*), and ferritin (*green*). Magnification, 200×. *Scale bar*: 25 µm. *$P < 0.05$, **$P < 0.01$, ***$P < 0.001$, ****$P < 0.0001$ versus the control group.

sis (Fig. 3B). Further analysis showed that induction of ferroptosis led to a significant increase in the expression of fibrosis-associated proteins, whereas inhibition of ferroptosis led to their decrease (Fig. 4). These findings suggest that SiO may influence HTMC fibrosis through regulation of ferroptosis, highlighting a potential mechanism by which SiO contributes to changes in the trabecular meshwork.

SiO Increases Ferroptosis and ROS Levels in HTMCs Through Upregulation of NOX4

Although previous data have established the role of SiO in promoting HTMC fibrosis through enhanced ferroptosis, the upstream mechanisms involved have remained unclear. Extensive research indicates that the ROS/NOX4/Smad3 pathway is intimately associated with HTMC fibrosis and implicated in the pathogenesis of open-angle glaucoma. This led us to hypothesize that this signaling axis mediates the effects of SiO on fibrosis and ferroptosis in HTMCs. To investigate this hypothesis, we examined NOX4 protein levels in HTMCs after SiO exposure. Additionally, we assessed changes in ferroptosis and ROS production following NOX4 knockdown. Our findings revealed that SiO treatment upregulated NOX4 protein expression and ROS levels in HTMCs (Figs. 5A, 5D). Conversely, NOX4 suppression markedly reduced ROS production and ferroptosis levels in HTMCs (Figs. 5B–F). Moreover, SiO treatment significantly elevated phosphorylated Smad3 (p-Smad3) levels without altering total Smad3 levels (Fig. 5B). The upregulation of p-Smad3 induced by SiO was attenuated following NOX4 inhibition (Fig. 5B). These results suggest that SiO-induced ferroptosis in HTMCs is mediated through

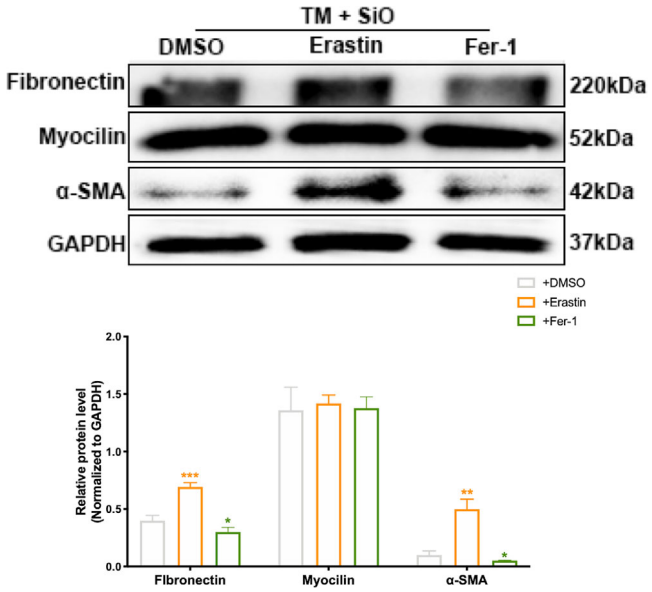

Figure 4. Protein expression of fibronectin ($P = 0.0006$ and $P = 0.0225$), myocilin ($P = 0.6586$ and $P = 0.8944$), and α-SMA ($P = 0.0018$ and $P = 0.0435$) in HTMCs treated with 20% SiO and erastin/Fer-1, respectively ($n = 3$). *$P < 0.05$, **$P < 0.01$, ***$P < 0.001$, ****$P < 0.0001$ versus the control group.

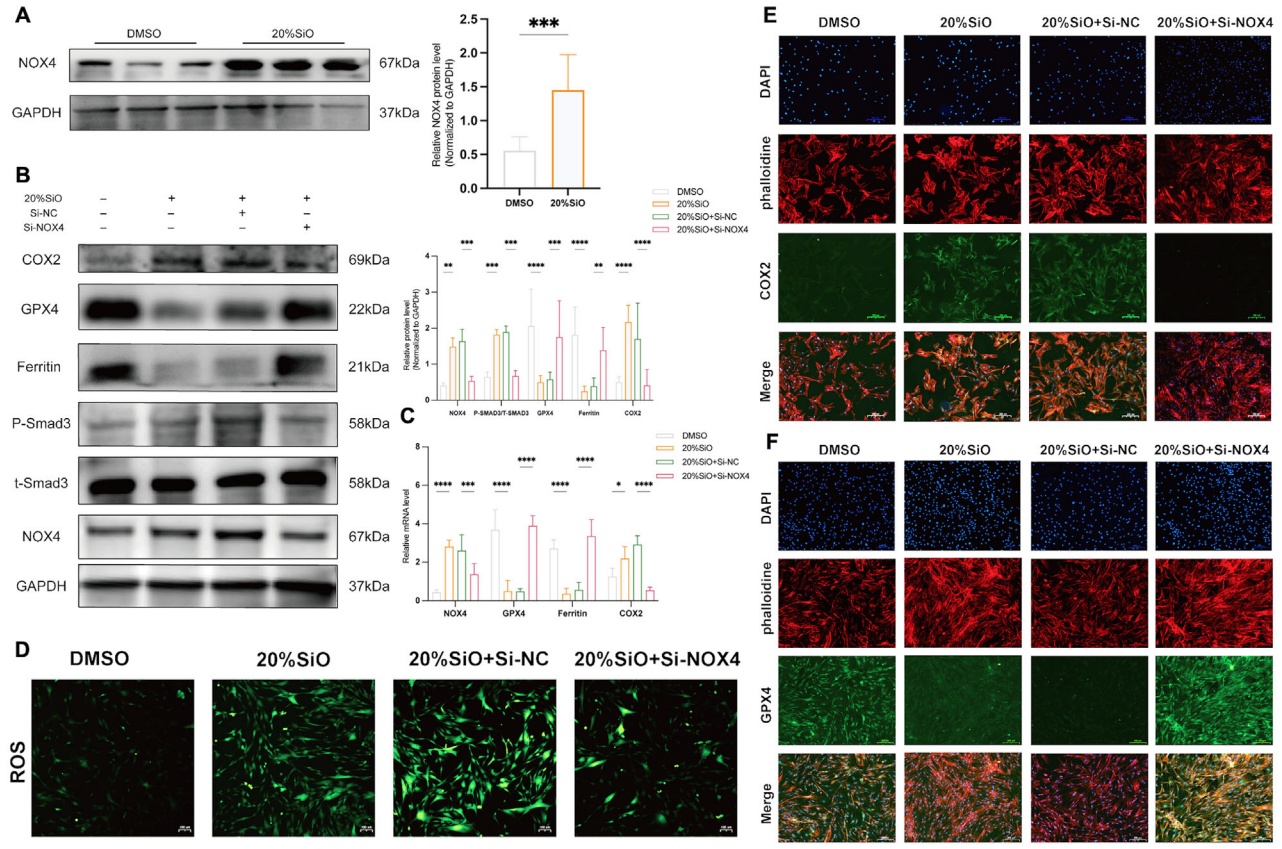

Figure 5. Effect of NOX4 on the modulation of ferroptosis and Smad3 phosphorylation levels. (**A**) Protein expression of NOX4 ($P = 0.0002$) in HTMCs treated with SiO ($n = 3$). (**B**) Protein expression of NOX4 ($P = 0.0013$ and $P = 0.0009$), COX2 ($P < 0.0001$ and $P < 0.0001$), GPX4 ($P < 0.0001$ and $P = 0.0003$), ferritin ($P < 0.0001$ and $P = 0.0055$), p-Smad3 ($P = 0.0003$ and $P = 0.0001$), and total Smad3 (t-Smad3) in HTMCs across control, SiO, SiO+small interfering RNA negative control (Si-NC), and SiO+Si-NOX4 groups ($n = 3$). (**C**) mRNA expression of NOX4 ($P < 0.0001$ and $P = 0.0006$), COX2 ($P = 0.0356$ and $P < 0.0001$), GPX4 ($P < 0.0001$ and $P < 0.0001$), and ferritin ($P < 0.0001$ and $P < 0.0001$) in HTMCs across control, SiO, SiO+Si-NC, and SiO+Si-NOX4 groups ($n = 3$). (**D**) Labeling of ROS in HTMCs of control, SiO, SiO+Si-NC, and SiO+Si-NOX4 groups. (**E**) Labeling of COX2 in HTMCs across control, SiO, SiO+Si-NC, and SiO+Si-NOX4 groups. Representative images depict the immunohistochemistry for HTMCs labeled by DAPI (*blue*), phalloidin (*red*), and COX2 (*green*). (**F**) Labeling of GPX4 in HTMCs across control, SiO, SiO+Si-NC, and SiO+Si-NOX4 groups. Representative images depict the immunohistochemistry for HTMCs labeled by DAPI (*blue*), phalloidin (*red*), and GPX4 (*green*). Magnification, 200×. *Scale bar*: 25 µm. *$P < 0.05$, **$P < 0.01$, ***$P < 0.001$, ****$P < 0.0001$ (P = DMSO vs. 20%SiO and P = 20%SiO+Si-NC vs. 20%SiO+Si-NOX4).

NOX4 activation, with potential involvement of Smad3 activation.

SiO Induces Ferroptosis and ROS Levels in HTMCs Via Smad3 Activation

To further confirm that Smad3 signaling is pivotal in promoting ferroptosis in HTMCs, we introduced the Smad3 inhibitor, SIS3, to examine its effects on ferroptosis and ROS levels in HTMCs treated with SiO. Consistent with our hypothesis, SIS3 significantly mitigated the enhanced ferroptosis and ROS levels induced by SiO (Fig. 6). These results suggest that SiO escalates ROS production in HTMCs by upregulating NOX4 and activating Smad3 signaling, thereby augmenting ferroptosis levels, which in turn contributes to the increased expression of fibrosis-related proteins in HTMCs.

Collectively, these results suggest that SiO influences the proliferation and fibrosis of human HTMCs through the induction of ferroptosis. This regulatory effect is mediated by the ROS/NOX4/Smad3 axis (Fig. 7), potentially elucidating the mechanism underlying the increase in intraocular pressure observed following SiO vitreous cavity filling.

Discussion

Physical and Chemical Properties of SiO

SiO plays a crucial role in vitreoretinal surgery, primarily serving as an intraocular tamponade. This intervention is pivotal in the landscape of ophthalmic surgical management, largely due to the unique physicochemical characteristics of SiO, which include a slightly lower specific gravity, low interfacial tension, and high viscosity, making it highly suitable for surgical applications.[1,38,39] Despite its relatively recent introduction to ophthalmic surgery compared to gases, with U.S. Food and Drug Administration (FDA) approval granted in 1996, the usage of SiO has expanded significantly. It is predominantly indicated for managing retinal detachments caused by varied etiologies such as proliferative vitreoretinopathy, viral retinitis, trauma, severe proliferative diabetic retinopathy, and high myopia.[40–43] Clinically, SiO is valued for its ability to provide sustained support to the heal-

Investigative Ophthalmology & Visual Science

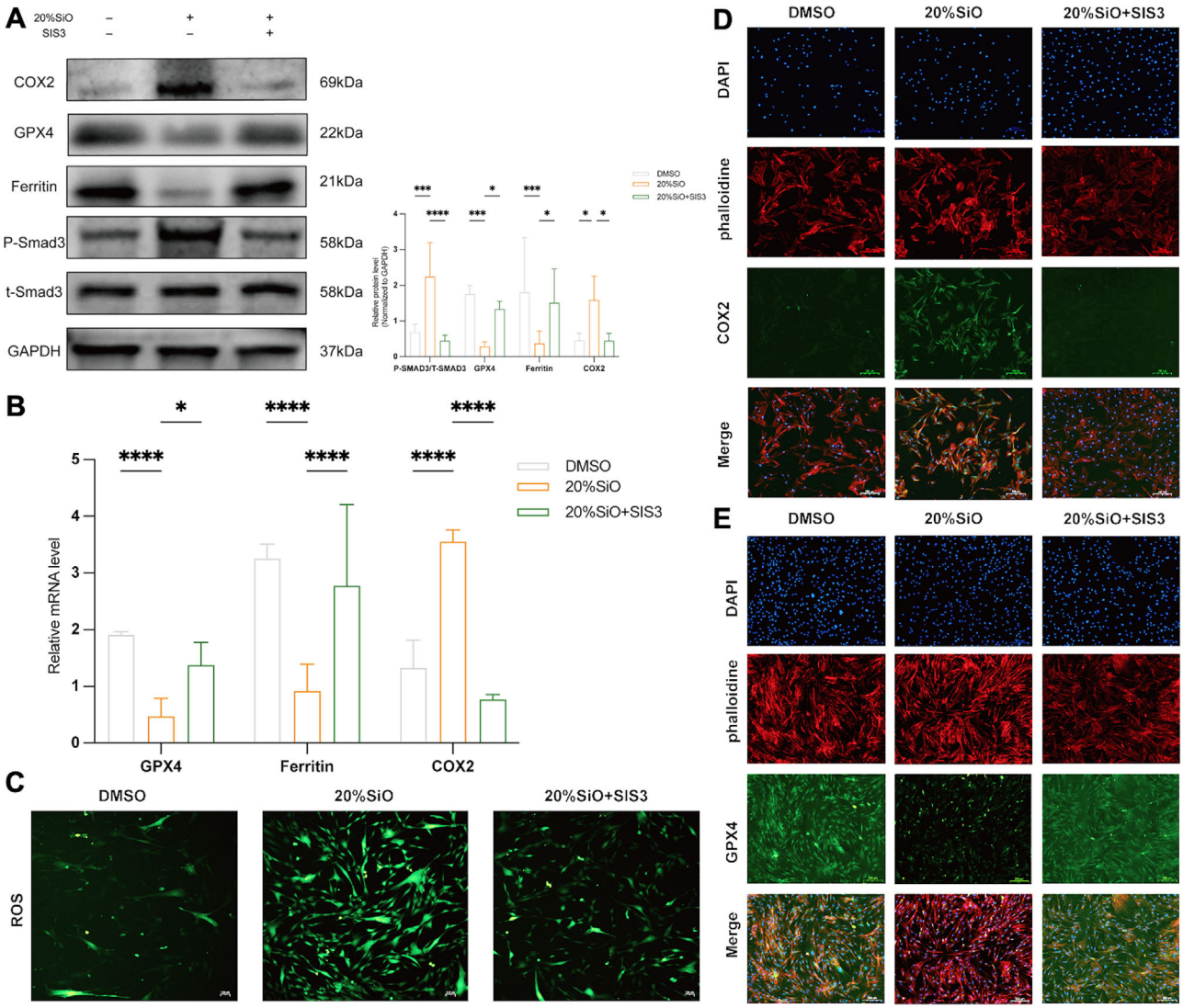

Figure 6. Effect of SIS3 on the modulation of ferroptosis and Smad3 phosphorylation levels. (**A**) Protein expression of COX2 ($P = 0.0179$ and $P = 0.0159$), GPX4 ($P = 0.0003$ and $P = 0.0396$), ferritin ($P = 0.0005$ and $P = 0.0157$), p-Smad3 ($P = 0.0001$ and $P < 0.0001$), and t-Smad3 in HTMCs across control, SiO, and SiO+SIS3 ($n = 3$). (**B**) mRNA expression of COX2 ($P < 0.0001$ and $P < 0.0001$), GPX4 ($P < 0.0001$ and $P = 0.0316$), and ferritin ($P < 0.0001$ and $P < 0.0001$) in HTMCs across control, SiO, and SiO+SIS3 ($n = 3$). (**C**) Labeling of ROS and HTMCs across control and SiO, SiO+SIS3. (**D**) Labeling of COX2 in HTMCs across control and SiO, SiO+SIS3. Representative images depict the immunohistochemistry for HTMCs labeled by DAPI (*blue*), phalloidin (*red*), and COX2 (*green*). (**E**) Labeling of GPX4 and HTMCs across control, SiO, and SiO+SIS3. Representative images depict the immunohistochemistry for HTMCs labeled by DAPI (*blue*), phalloidin (*red*), and GPX4 (*green*). Magnification 200×. *Scale bar*: 25 µm. *$P < 0.05$, **$P < 0.01$, ***$P < 0.001$, ****$P < 0.0001$ (P = DMSO vs. 20%SiO and P = 20%SiO vs. 20%SiO+Si-SIS3).

ing retina. Nonetheless, there has been an increasing number of reports of visual impairments associated with SiO,[44–47] prompting a reevaluation of its necessity in certain surgical contexts.[48]

SiO Complications and SiO-Related Visual Loss

Cataract and glaucoma are the predominant complications associated with long-term SiO tamponade. These complications are often linked to the emulsification and intraocular migration of SiO, phenomena that are challenging to prevent. As SiO has become more widely utilized, the term silicone oil–related visual loss (SORVL) has been introduced, raising concerns regarding the safety of SiO use.[49] SORVL is characterized as severe visual loss exceeding 2 Snellen lines either during the period of SiO tamponade or at the time of its removal, in the absence of any clear alternative cause.[50] Although the exact etiology and incidence of SORVL remain elusive, proposed mechanisms include a limited potassium sink into the vitreous cavity, elevated concentrations of fibrotic growth factors in aged oil,[51] and phototoxic damage from ultraviolet light exposure, among others. Additionally, the duration of SiO tamponade is considered a risk factor for SORVL, leading to increased advocacy among ophthalmologists for the early removal of SiO. Given the inherent challenges in mitigating complications due to the physicochemical properties of SiO, several alternative materials, such as the foldable capsule vitreous body,[52] hydrogel biomaterials,[53] and medium-chain triglycerides,[54] have been explored. However, the clinical viability of these alternatives still requires extensive investigation.

Investigative Ophthalmology & Visual Science

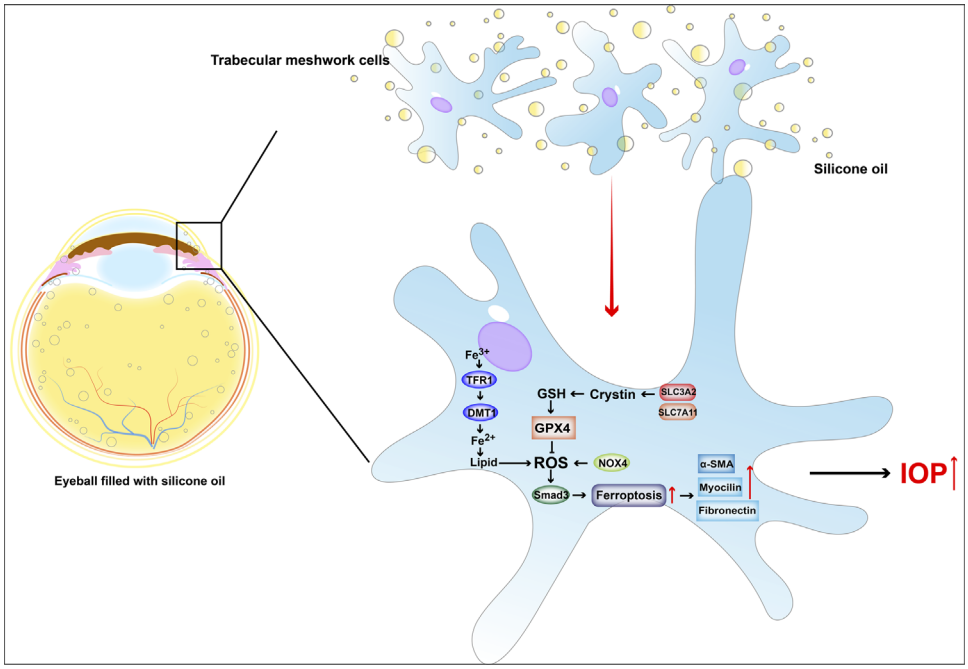

Figure 7. SiO influences fibrosis in HTMCs via ferroptosis induction. Following PPV and vitreous tamponade with SiO, SiO enters the anterior chamber and infiltrates HTMCs. It induces ferroptosis in HTMCs through the ROS/NOX4/Smad3 signaling pathway, ultimately promoting fibrosis of the HTMCs and contributing to the development of elevated IOP.

TMC Dysfunction and the Pathogenesis of Glaucoma

The TM plays a crucial role in regulating aqueous humor outflow from the anterior chamber, thus maintaining IOP through a balance between fluid production by the ciliary body and drainage via the TM.[17] Structurally, the TM consists of three distinct layers: the uveal meshwork, corneoscleral meshwork, and a specialized layer of TMCs.[55] Fibrosis of the TM, a pathological repair process characterized by the excessive deposition of ECM and proliferation of contractile myofibroblasts,[56–58] leads to persistent ECM buildup and structural distortion of the TM. This results in increased resistance to aqueous humor outflow and elevated IOP and ultimately contributes to the pathogenesis of POAG and the failure of minimally invasive glaucoma surgery devices.[59] This study uniquely determined that the increase in IOP induced by SiO is also likely to be linked to fibrosis of TMCs, with ferroptosis playing a critical role in this pathological process. In this study, we treated HTMCs with varying concentrations of SiO (0%–40%) and assessed cell viability, proliferation, fibrosis, and ferroptosis. The results demonstrated that 20% SiO significantly affected these parameters but increasing the concentration to 40% did not further enhance fibronectin expression. This suggests that 20% SiO represents a threshold concentration for inducing fibrotic changes, making it suitable for further mechanistic exploration.

Interestingly, the dose–response of SiO on fibronectin differed from that of other fibrotic markers. We hypothesize that this reflects the unique role of fibronectin in the early stages of fibrosis. As an ECM organizer, fibronectin is one of the first markers to respond to tissue injury, serving as a scaffold for collagen deposition.[60] In contrast, markers such as actin and α-SMA are more associated with specific fibrotic conditions and the later stages of fibrosis.[61,62] At lower SiO concentrations (<20%), fibronectin upregulation suggests early fibrotic changes, whereas its reduction at higher concentrations (40%) may indicate late-stage cellular damage, with fibronectin synthesis being particularly sensitive to these effects.

Additionally, we observed that ferritin levels did not show significant changes across SiO concentrations. Ferritin regulates iron storage and mitigates oxidative stress by sequestering iron, preventing ROS formation and lipid peroxidation—key events in ferroptosis.[63] Unlike other ferroptosis markers, such as ACSL4, COX2, and GPX4, which are directly involved in lipid metabolism and oxidative stress, ferritin plays a central role in iron homeostasis.[64,65] As a result, its levels may exhibit less variability. At lower SiO concentrations (<20%), compensatory ferritin synthesis may protect cells from ferroptosis; however, at higher concentrations (>20%), this protective mechanism may become insufficient, leading to decreased ferritin levels. These findings offer new insights into the mechanisms underlying SiO-related complications and suggest potential therapeutic targets for managing these adverse effects.

Oxidative Stress in TMCs and the Pathogenesis of Glaucoma

Oxidative stress is a well-established factor in the pathology of numerous neurodegenerative diseases and is similarly recognized as a critical contributor to the pathophysiology of POAG.[66,67] Prior research has demonstrated elevated levels of oxidative stress markers in the aqueous humor of patients with POAG.[35,68] Additionally, significant alterations in the expression of antioxidative enzymes such as superoxide dismutase, catalase, and glutathione have been observed in the TM of glaucoma patients.[69,70] Furthermore,

selective oxidative damage to TM mitochondria induced by free radicals and ROS may precipitate TM cell dysfunction.[71] The findings of our current study suggest that the ROS/NOX4/Smad3 signaling axis plays a role in regulating ferroptosis levels in TM cells, corroborating previous research and underscoring how oxidative stress significantly impacts TM cellular function. Moreover, involvement of the ROS/NOX4/Smad3 axis has been reported in the pathogenesis of aging and open-angle glaucoma,[72,73] aligning with the results of this study.

This study is not without limitations. The experimental scope was confined to HTMCs, and the research occurred at the cellular level, thus lacking in vivo experimental validation. The methodology for developing animal models of SiO anterior chamber angle infiltration remains underdeveloped. We intend to continue monitoring advancements in relevant animal models and aim to enhance our experimental designs with animal studies as opportunities arise. Additionally, although this research emphasized SiO-induced ferroptosis in HTMCs, it is important to acknowledge that the increase in IOP associated with SiO may involve other mechanisms. These include the viscosity and chemical composition of SiO, which could obstruct the trabecular meshwork, alter aqueous humor dynamics, and affect retinal and choroidal vascular permeability.[10,74,75] Furthermore, the inflammatory response elicited by SiO may contribute to fibrosis in the outflow pathway, potentially exacerbating IOP.[4] These aspects warrant further investigation.

Acknowledgments

Supported by grants from the National Natural Science Foundation of China (82070953, 82371048, 82000885), the Shanghai Science and Technology Committee Project Foundation (21Y11909700), and the China Postdoctoral Science Foundation (2024M762024).

Data Availability and Materials: The datasets used and/or analyzed during the current study are available from the corresponding author on reasonable request.

Disclosure: **J. Wang**, None; **Y. Zhang**, None; **H. Zhong**, None; **Y. Zhang**, None; **R. Han**, None; **Y. Guo**, None; **S. Huang**, None; **H. Yu**, None; **Y. Zhong**, None

References

1. Barca F, Caporossi T, Rizzo S. Silicone oil: different physical proprieties and clinical applications. *Biomed Res Int*. 2014;2014:502143.
2. Cibis PA, Becker B, Okun E, Canaan S. The use of liquid silicone in retinal detachment surgery. *Arch Ophthalmol*. 1962;68:590–599.
3. Budenz DL, Taba KE, Feuer WJ, et al. Surgical management of secondary glaucoma after pars plana vitrectomy and silicone oil injection for complex retinal detachment. *Ophthalmology*. 2001;108:1628–1632.
4. Nicolai M, Lassandro N, Franceschi A, et al. Intraocular pressure rise linked to silicone oil in retinal surgery: a review. *Vision (Basel)*. 2020;4:36.
5. Riedel KG, Gabel VP, Neubauer L, Kampik A, Lund OE. Intravitreal silicone oil injection: complications and treatment of 415 consecutive patients. *Graefes Arch Clin Exp Ophthalmol*. 1990;228:19–23.
6. Spiegel D, Nasemann J, Nawrocki J, Gabel VP. Severe ocular trauma managed with primary pars plana vitrectomy and silicone oil. *Retina*. 1997;17:275–285.
7. Pang MP, Peyman GA, Kao GW. Early anterior segment complications after silicone oil injection. *Can J Ophthalmol*. 1986;21:271–275.
8. Honavar SG, Goyal M, Majji AB, Sen PK, Naduvilath T, Dandona L. Glaucoma after pars plana vitrectomy and silicone oil injection for complicated retinal detachments. *Ophthalmology*. 1999;106:169–176; discussion 177.
9. Jonas JB, Knorr HL, Rank RM, Budde WM. Intraocular pressure and silicone oil endotamponade. *J Glaucoma*. 2001;10:102–108.
10. Ichhpujani P, Jindal A, Jay Katz L. Silicone oil induced glaucoma: a review. *Graefes Arch Clin Exp Ophthalmol*. 2009;247:1585–1593.
11. Pavlidis M, Scharioth G, de Ortueta D, Baatz H. Iridolenticular block in heavy silicone oil tamponade. *Retina*. 2010;30:516–520.
12. Vela JI, Crespí J, Díaz-Cascajosa J, Buil JA. Pupillary block glaucoma in phakic eyes using 5000 centistoke silicone oil. *Retin Cases Brief Rep*. 2009;3:96–98.
13. Jackson TL, Thiagarajan M, Murthy R, Snead MP, Wong D, Williamson TH. Pupil block glaucoma in phakic and pseudophakic patients after vitrectomy with silicone oil injection. *Am J Ophthalmol*. 2001;132:414–416.
14. Al-Jazzaf AM, Netland PA, Charles S. Incidence and management of elevated intraocular pressure after silicone oil injection. *J Glaucoma*. 2005;14:40–46.
15. Tektas OY, Lütjen-Drecoll E. Structural changes of the trabecular meshwork in different kinds of glaucoma. *Exp Eye Res*. 2009;88:769–775.
16. Buffault J, Labbé A, Hamard P, Brignole-Baudouin F, Baudouin C. The trabecular meshwork: structure, function and clinical implications. A review of the literature. *J Fr Ophtalmol*. 2020;43:e217–e230.
17. Vranka JA, Kelley MJ, Acott TS, Keller KE. Extracellular matrix in the trabecular meshwork: intraocular pressure regulation and dysregulation in glaucoma. *Exp Eye Res*. 2015;133:112–125.
18. Stamer WD, Clark AF. The many faces of the trabecular meshwork cell. *Exp Eye Res*. 2017;158:112–123.
19. Acott TS, Kelley MJ. Extracellular matrix in the trabecular meshwork. *Exp Eye Res*. 2008;86:543–561.
20. Zheng J, Conrad M. The metabolic underpinnings of ferroptosis. *Cell Metab*. 2020;32:920–937.
21. Stockwell BR, Friedmann Angeli JP, Bayir H, et al. Ferroptosis: a regulated cell death nexus linking metabolism, redox biology, and disease. *Cell*. 2017;171:273–285.
22. Brown CW, Amante JJ, Chhoy P, et al. Prominin2 drives ferroptosis resistance by stimulating iron export. *Dev Cell*. 2019;51:575–586.e4.
23. Brown CW, Amante JJ, Goel HL, Mercurio AM. The $\alpha 6\beta 4$ integrin promotes resistance to ferroptosis. *J Cell Biol*. 2017;216:4287–4297.
24. Dodson M, Castro-Portuguez R, Zhang DD. NRF2 plays a critical role in mitigating lipid peroxidation and ferroptosis. *Redox Biol*. 2019;23:101107.
25. Han C, Liu Y, Dai R, Ismail N, Su W, Li B. Ferroptosis and its potential role in human diseases. *Front Pharmacol*. 2020;11:239.
26. Cui Y, Zhang Y, Zhao X, et al. ACSL4 exacerbates ischemic stroke by promoting ferroptosis-induced brain injury and neuroinflammation. *Brain Behav Immun*. 2021;93:312–321.
27. Yao F, Peng J, Zhang E, et al. Pathologically high intraocular pressure disturbs normal iron homeostasis and leads to retinal ganglion cell ferroptosis in glaucoma. *Cell Death Differ*. 2023;30:69–81.
28. Tang J, Zhuo Y, Li Y. Effects of iron and zinc on mitochondria: potential mechanisms of glaucomatous injury. *Front Cell Dev Biol*. 2021;9:720288.

29. Gye HJ, Kim JM, Yoo C, et al. Relationship between high serum ferritin level and glaucoma in a South Korean population: the Kangbuk Samsung health study. *Br J Ophthalmol*. 2016;100:1703–1707.
30. Ramdas WD. The relation between dietary intake and glaucoma: a systematic review. *Acta Ophthalmol*. 2018;96:550–556.
31. Zhu J, Chen H, Wu J, et al. Ferroptosis in glaucoma: a promising avenue for therapy. *Adv Biol (Weinh)*. 2024;8:e2300530.
32. Xue W, Comes N, Borrás T. Presence of an established calcification marker in trabecular meshwork tissue of glaucoma donors. *Invest Ophthalmol Vis Sci*. 2007;48:3184–3194.
33. Pattabiraman PP, Rao PV. Mechanistic basis of Rho GTPase-induced extracellular matrix synthesis in trabecular meshwork cells. *Am J Physiol Cell Physiol*. 2010;298:C749–C763.
34. Pattabiraman PP, Maddala R, Rao PV. Regulation of plasticity and fibrogenic activity of trabecular meshwork cells by Rho GTPase signaling. *J Cell Physiol*. 2014;229:927–942.
35. Goyal A, Srivastava A, Sihota R, Kaur J. Evaluation of oxidative stress markers in aqueous humor of primary open angle glaucoma and primary angle closure glaucoma patients. *Curr Eye Res*. 2014;39:823–829.
36. Pinazo-Duran MD, Shoaie-Nia K, Zanón-Moreno V, Sanz-González SM, del Castillo JB, García-Medina JJ. Strategies to reduce oxidative stress in glaucoma patients. *Curr Neuropharmacol*. 2018;16:903–918.
37. Pfaffl MW. A new mathematical model for relative quantification in real-time RT-PCR. *Nucleic Acids Res*. 2001;29:e45.
38. Foster WJ. Vitreous substitutes. *Expert Rev Ophthalmol*. 2008;3:211–218.
39. Joussen AM, Wong D. The concept of heavy tamponades—chances and limitations. *Graefes Arch Clin Exp Ophthalmol*. 2008;246:1217–1224.
40. Ortisi E, Avitabile T, Bonfiglio V. Surgical management of retinal detachment because of macular hole in highly myopic eyes. *Retina*. 2012;32:1704–1718.
41. Nadal J, Verdaguer P, Canut MI. Treatment of retinal detachment secondary to macular hole in high myopia: vitrectomy with dissection of the inner limiting membrane to the edge of the staphyloma and long-term tamponade. *Retina*. 2012;32:1525–1530.
42. Azen SP, Scott IU, Flynn HW, Jr, et al. Silicone oil in the repair of complex retinal detachments. A prospective observational multicenter study. *Ophthalmology*. 1998;105:1587–1597.
43. Pastor JC. Proliferative vitreoretinopathy: an overview. *Surv Ophthalmol*. 1998;43:3–18.
44. Ghoraba HH, Zaky AG, Heikal MA, Elgemai EEM, Abd Al Fatah HM. Silicone oil-related visual loss. *Ophthalmologica*. 2017;238:59–67.
45. Ting MYL, Kim SE, Anguita R. Endophthalmitis in silicone oil-filled eyes. *Antibiotics (Basel)*. 2023;12:736.
46. Okonkwo ON, Hassan AO, Oderinlo O, Gyasi ME. *Burkholderia cepacia*, a cause of post pars plana vitrectomy silicone oil related endophthalmitis: clinico-pathological presentation and outcome of management. *Int J Retina Vitreous*. 2018;4:35.
47. Barth T, Helbig H, Maerker D, Gamulescu MA, Radeck V. Unexplained visual loss after primary pars-plana-vitrectomy with silicone oil tamponade in fovea-sparing retinal detachment. *BMC Ophthalmol*. 2023;23:75.
48. Pieczynski J, Kuklo P, Grzybowski A. Pars plana vitrectomy with silicone oil tamponade for primary and secondary macular hole closure: is it still a useful procedure? *Eur J Ophthalmol*. 2018;28:503–514.
49. Chen Y, Kearns VR, Zhou L, et al. Silicone oil in vitreoretinal surgery: indications, complications, new developments and alternative long-term tamponade agents. *Acta Ophthalmol*. 2021;99:240–250.
50. Scheerlinck LM, Schellekens PA, Liem AT, Steijns D, Leeuwen R. Incidence, risk factors, and clinical characteristics of unexplained visual loss after intraocular silicone oil for macula-on retinal detachment. *Retina*. 2016;36:342–350.
51. Asaria RH, Kon CH, Bunce C, et al. Silicone oil concentrates fibrogenic growth factors in the retro-oil fluid. *Br J Ophthalmol*. 2004;88:1439–1442.
52. Lin X, Wang Z, Jiang Z, et al. Preliminary efficacy and safety of a silicone oil-filled foldable capsular vitreous body in the treatment of severe retinal detachment. *Retina*. 2012;32:729–741.
53. Spang MT, Christman KL. Extracellular matrix hydrogel therapies: in vivo applications and development. *Acta Biomater*. 2018;68:1–14.
54. Soler VJ, Laurent C, Sakr F, et al. Preliminary study of the safety and efficacy of medium-chain triglycerides for use as an intraocular tamponading agent in minipigs. *Graefes Arch Clin Exp Ophthalmol*. 2017;255:1593–1604.
55. Tamm ER. The trabecular meshwork outflow pathways: structural and functional aspects. *Exp Eye Res*. 2009;88:648–655.
56. O'Regan A, O'Brien CJ, Eivers SB. The lysophosphatidic acid axis in fibrosis: implications for glaucoma. *Wound Repair Regen*. 2021;29:613–626.
57. Henderson NC, Rieder F, Wynn TA. Fibrosis: from mechanisms to medicines. *Nature*. 2020;587:555–566.
58. Gauthier AC, Liu J. Epigenetics and signaling pathways in glaucoma. *Biomed Res Int*. 2017;2017:5712341.
59. Qin M, Yu-Wai-Man C. Glaucoma: novel antifibrotic therapeutics for the trabecular meshwork. *Eur J Pharmacol*. 2023;954:175882.
60. Singh P, Carraher C, Schwarzbauer JE. Assembly of fibronectin extracellular matrix. *Annu Rev Cell Dev Biol*. 2010;26:397–419.
61. Faralli JA, Filla MS, Peters DM. Role of integrins in the development of fibrosis in the trabecular meshwork. *Front Ophthalmol (Lausanne)*. 2023;3:1274797.
62. Kim KK, Sheppard D, Chapman HA. TGF-β1 signaling and tissue fibrosis. *Cold Spring Harb Perspect Biol*. 2018;10:a022293.
63. Tang D, Chen X, Kang R, Kroemer G. Ferroptosis: molecular mechanisms and health implications. *Cell Res*. 2021;31:107–125.
64. Torti FM, Torti SV. Regulation of ferritin genes and protein. *Blood*. 2002;99:3505–3516.
65. Chen X, Li J, Kang R, Klionsky DJ, Tang D. Ferroptosis: machinery and regulation. *Autophagy*. 2021;17:2054–2081.
66. Zhao J, Wang S, Zhong W, Yang B, Sun L, Zheng Y. Oxidative stress in the trabecular meshwork (review). *Int J Mol Med*. 2016;38:995–1002.
67. Izzotti A, Bagnis A, Saccà SC. The role of oxidative stress in glaucoma. *Mutat Res*. 2006;612:105–114.
68. Ferreira SM, Lerner SF, Brunzini R, Evelson PA, Llesuy SF. Oxidative stress markers in aqueous humor of glaucoma patients. *Am J Ophthalmol*. 2004;137:62–69.
69. Majsterek I, Malinowska K, Stanczyk M, et al. Evaluation of oxidative stress markers in pathogenesis of primary open-angle glaucoma. *Exp Mol Pathol*. 2011;90:231–237.
70. Ghanem AA, Arafa LF, El-Baz A. Oxidative stress markers in patients with primary open-angle glaucoma. *Curr Eye Res*. 2010;35:295–301.
71. Tripathi RC, Li J, Chan WF, Tripathi BJ. Aqueous humor in glaucomatous eyes contains an increased level of TGF-β2. *Exp Eye Res*. 1994;59:723–727.

Investigative Ophthalmology & Visual Science

72. Li H, Ren J, Cui H, et al. Dexamethasone induces senescence-associated changes in trabecular meshwork cells by increasing ROS levels via the TGFβ/Smad3-NOX4 axis. *Cell Transplant*. 2023;32:9636897231177356.
73. Li H, Cui H, Ren J, et al. Elevated Angiotensin-II levels contribute to the pathogenesis of open-angle glaucoma via inducing the expression of fibrosis-related genes in trabecular meshwork cells through a ROS/NOX4/SMAD3 axis. *Cell Transplant*. 2023;32:9636897231162526.
74. Ge L, Su N, Fan W, Yuan S. Risk factors and management of intraocular pressure elevation after vitrectomy combined with silicone oil tamponade. *Int J Gen Med*. 2024;17:447–456.
75. Chen J, Guan L, Liu Y, et al. Choroidal vascular changes in silicone oil-filled eyes after vitrectomy for rhegmatogenous retinal detachments. *BMC Ophthalmol*. 2023;23:442.

Investigative Ophthalmology & Visual Science